Scientific Research Publishing

Advances in Materials Physics and Chemistry, 2017, 7, 223-241
http://www.scirp.org/journal/ampc
ISSN Online: 2162-5328
ISSN Print: 2162-531X

# Thermal Behavior and Magnetic Properties of Nd-Fe-B Based Exchange Spring Nanocomposites $Nd_{4-x}Tb_xFe_{83.5}Co_5Cu_{0.5}Nb_1B_6$ (x = 0, 0.2, 0.4, 0.6, 0.8 and 1) Melt-Spun Ribbons

**Palash Chandra Karmaker[1,2*], Mohammad Obaidur Rahman[2], Nguyen Huy Dan[3], Samia Islam Liba[1], Per Nordblad[4], Dilip Kumar Saha[1], Sheikh Manjura Hoque[1]**

[1]Materials Science Division, Atomic Energy Center, Dhaka, Bangladesh
[2]Department of Physics, Jahangirnagar University, Dhaka, Bangladesh
[3]Institute of Materials Science, Vietnam Academy of Science and Technology, Hanoi, Vietnam
[4]Solid State Physics, Department of Engineering Science, Uppsala University, Uppsala, Sweden
Email: *pckarmakerpu@gmail.com

**How to cite this paper:** Karmaker, P.C., Rahman, M.O., Dan, N.H., Liba, S.I., Nordblad, P., Saha, D.K. and Hoque, S.M. (2017) Thermal Behavior and Magnetic Properties of Nd-Fe-B Based Exchange Spring Nanocomposites $Nd_{4-x}Tb_xFe_{83.5}Co_5Cu_{0.5}Nb_1B_6$ (x = 0, 0.2, 0.4, 0.6, 0.8 and 1) Melt-Spun Ribbons. *Advances in Materials Physics and Chemistry*, **7**, 223-241.
https://doi.org/10.4236/ampc.2017.76018

**Received:** April 20, 2017
**Accepted:** June 9, 2017
**Published:** June 12, 2017



## Abstract

Co-rich Nd-Fe-B nanocomposite ribbons with Tb substituted have been fabricated by single roller melt spinning technique of $Nd_{4-x}Tb_xFe_{83.5}Co_5Cu_{0.5}Nb_1B_6$ (x = 0, 0.2, 0.4, 0.6, 0.8 and 1) alloys in an argon (Ar) atmosphere at a circumferential speed of 40 m/s. According to the differential scanning calorimeter (DSC) traces the nanocomposite samples have been annealed at different temperatures like 675˚C, 687˚C, 700 ˚C, 712˚C and 725˚C for 10 min. Crystallization behavior was studied by X-ray diffraction in which it was found that the XRD patterns are characterized by broad diffused pattern which demonstrate the amorphous state of materials. The ribbon samples were also characterized by vibration sample magnetometer (VSM) and Mössbauer spectroscopy at as-cast and annealed condition. Co-rich and Tb substitution has significantly enhanced the value of coercivity ($H_c$) and maximum energy product $(BH)_{max}$. Highest value of $H_c$ and $(BH)_{max}$ has been obtained as 2.36 kOe and 6.11 MGOe for the sample annealed at 700˚C for 10 min with higher concentration of Tb. The M-H hysteresis loops show extremely soft natures which do not possess any area. We have found reduced remanent ratio ($M_r/M_s$) up to 0.49 at optimal annealing temperature 700˚C. However, with the annealing of the samples in the above mentioned temperature, evolution of large coercivity was observed due to the formation of exchange couple hard and soft nanocrystal composites. We have investigated the variation of Curie temperature ($T_c$) with annealing temperature of the melt

spun ribbon samples. Mossbauer spectroscopy was carried out to study the hyperfine parameters such as hyperfine field, hyperfine field distribution for full width half maximum (FWHM) and isomer shift of Fe species of these two phases.

## Keywords

Coercivity, Maximum Energy Product, Remanent Ratio, Nanocomposite, Hard and Soft Phases

## 1. Introduction

The Nd-Fe-B based nanocomposite materials, so-called exchange spring magnets, have attracted many scientists by virtue of their large potential in practical application [1]. These materials contain two main magnetic phases: the hard magnetic phase ($Nd_2Fe_{14}B$) and the soft magnetic phase ($Fe_3B$, $\alpha$-Fe), which are coupled via exchange interaction in nanometer scale. The ideal microstructure of the exchange spring magnets is formed by identical hard magnetic nanocrystallites homogeneously dispersed in a soft magnetic matrix [2]. The exchange spring effect between the hard and soft magnetic phases allows combining both the high coercivity of the hard magnetic phase and the high saturation magnetization of the soft magnetic phase leading to high maximum energy product of the material. There are two ways to control the formation of the nanocrystallites in the alloys prepared by melt spinning method. The first way is based on the variation of the annealing conditions for the alloys, which are amorphous in the as-quenched state. The second way is based on the change of the quenching rate of the melted alloys. The optimal annealing condition or quenching rate depends on the composition of the alloy. The problems of the undoped Nd-Fe-B exchange spring magnets are rather low Curie temperature and coercivity. Besides that, the sensitivity of the structure of the materials with the fabrication conditions is also another problem. The addition of elements such as Tb, Dy, Gd, Pr, Nb, Cu, Co, Cr ... is one of the means to improve the parameters of the hard magnetic behavior and fabrication technology of the material [3] [4] [5] [6]. In order to control the formation of the crystallites in the Fe-based magnetic materials, Nb is commonly added to the materials because Nb can surround the crystallites and prevent the growth of the crystallites. One of the problems of the Nd-Fe-B based exchange spring magnetic system is the formation of the large crystallites, which degrade the exchange spring effect and reduce coercivity of the material. The crystallites in this kind of materials can be refined by Nb-addition. With an appropriate concentration of Nb, the crystallites can be formed more identically in nanometer scale improving exchange spring effect and the coercivity can be enhanced due to the separation of the magnetic crystallites by Nb-boundaries. These lead to better performance of the Nd-Fe-B based exchange spring magnets. In other hand, Nb can reduce the critical quenching rate and the fabrication condition sensitivity, which have important significant meaning in

practical production of the material. To enhance Curie temperature of the material, the addition of cobalt (Co) is the most suitable and can improve coercivity and remanence of the material too [4]. In our present investigation, we have chosen the composition of $Nd_{4-x}Tb_xFe_{83.5}Co_5Cu_{0.5}Nb_1B_6$ (x = 0, 0.2, 0.4, 0.6, 0.8 and 1) to investigate thoroughly the evolution of different phases and its correlation with magnetic properties with the variation of annealing temperatures and times.

## 2. Experiments

An ingot of composition $Nd_{4-x}Tb_xFe_{83.5}Co_5Cu_{0.5}Nb_1B_6$ (x = 0, 0.2, 0.4, 0.6, 0.8 and 1) was prepared by arc melting the constituent elements in an argon atmosphere. The purity and origin of the materials were Nd (99.9%), Tb (99.9%), Fe (99.98%), Cu (99%), Nb (99.8%) and B (99.5%) from Johnson Matthey (Alfa Aesar) and Co (99.8%) from Chempur Feinchemikalien. Amorphous ribbons were prepared from the ingot using a melt-spin machine with a wheel speed of 40 m/s in an Ar atmosphere. The resulting ribbons were heat treated in an evacuated quartz tube of $10^{-5}$ mbar pressure at different temperatures and times to observe the effect of annealing condition on the magnetic properties. Differential scanning calorimetry was used to determine the crystallization temperature and X-ray diffraction ($CuK_\alpha$) was used to identify the phases present in the samples at different stages of the crystallization process. Magnetization measurements were performed in a vibrating sample magnetometer (Model: EV9 of micro Sense, USA). Curie temperature was derived from the differentiation of temperature dependence magnetization. $^{57}Fe$ Mössbauer spectrometer in transmission geometry was used with constant acceleration mode, using a $^{57}Fe$ source diffused in a rhodium matrix. The Mössbauer measurements were carried out in the conventional transmission mode at room temperature.

## 3. Results and Discussions

The crystallization temperatures of composition $Nd_{4-x}Tb_xFe_{83.5}Co_5Cu_{0.5}Nb_1B_6$ (x = 0, 0.2, 0.4, 0.6, 0.8 and 1) were identified by DSC. The DSC trace has been measured on nanocomposite ribbon samples in the as-cast condition by carrying out measurement in an argon atmosphere with a continuous heating rate of 10˚C/min, which are shown in **Figure 1**. The curves show exothermic peaks which represent the formation of metastable, hard and soft phases. Onset of crystallization of the first exothermic peak is at 454˚C for x = 0 while the peak temperature is at 491˚C and which at 520˚C fall in crystallization. For the second exothermic peak, initiation temperature of crystallization is 690˚C where the peak temperature is 712˚C. The second exothermic peak for x = 0 fall in crystallization at 720˚C, where the crystallization process is completed around 725˚C. For the sample x = 0.2, the initiation temperature of first exothermic peak is at 456˚C and the peak temperature is 495˚C, which at 525˚C fall in crystallization. The peak temperature for second exothermic peak is at 680˚C, where the initiation temperature is at 670˚C, while fall in crystallization is at 700˚C.

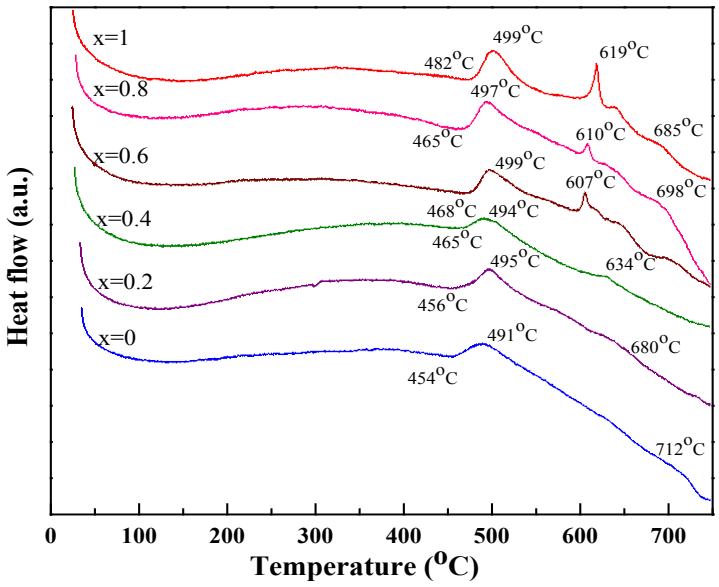


**Figure 1.** DSC trace of $Nd_{4-x}TbxFe_{83.5}Co_5Cu_{0.5}Nb_1B_6$ (x = 0, 0.2, 0.4, 0.6, 0.8 and 1) in the as-cast condition with a heating rate of 10˚C/min.

The whole crystallization process is also completed around 725˚C for x = 0.2. We have found that for x = 0.4, the peak temperatures of the first and second exothermic peaks are at 494˚C and 634˚C, initiation temperature are 465˚C and 610˚C. Fall in crystallization temperature for these two exothermic peaks are at 520˚C and 650˚C. Around 725˚C the crystallization process is completed for this composition. We have seen for x = 0.6, the peak temperatures of the first, second and third exothermic peaks are at 499˚C, 607˚C and 640˚C, initiation temperature are 468˚C, 590˚C and 625˚C. Fall in crystallization temperature for these three exothermic peaks are at 520˚C, 620˚C and 655˚C. The crystallization process is completed for this composition around at 725˚C. For the sample x = 0.8, the initiation temperature of first exothermic peak is at 465˚C and the peak temperature is 497˚C, which at 520˚C fall in crystallization. The peak temperatures for second and third exothermic peaks are at 610˚C and 698˚C, where the initiation temperatures are at 590˚C and 678˚C respectively. The temperature of fall in crystallization for second and third exothermic peaks is 625˚C and 715˚C respectively. The whole crystallization process is also completed around 725˚C for x = 0.8. We have seen for x = 1, the peak temperatures of the first, second, third and forth exothermic peaks are at 499˚C, 619˚C, 640˚C and 685˚C , initiation temperature are 492˚C, 598˚C, 630˚C, and 670˚C respectively. Fall in crystallization temperature for these three exothermic peaks are at 520˚C, 625˚C, 645˚C and 715˚C. Around at 725˚C, the crystallization process is fully completed for this composition. We can see that the exothermic peaks are gradually increased and sharpen for higher Tb concentration. Finally we have seen the overall crystallization process is completed within the range of 454˚C to 725˚C [7].

X-ray diffraction (XRD) studies have been performed to determine the phases. Diffraction patterns of the ribbon samples in the as-cast condition and annealed at 700˚C and 725˚C for 10 min as shown in **Figure 2**. We can see that all the

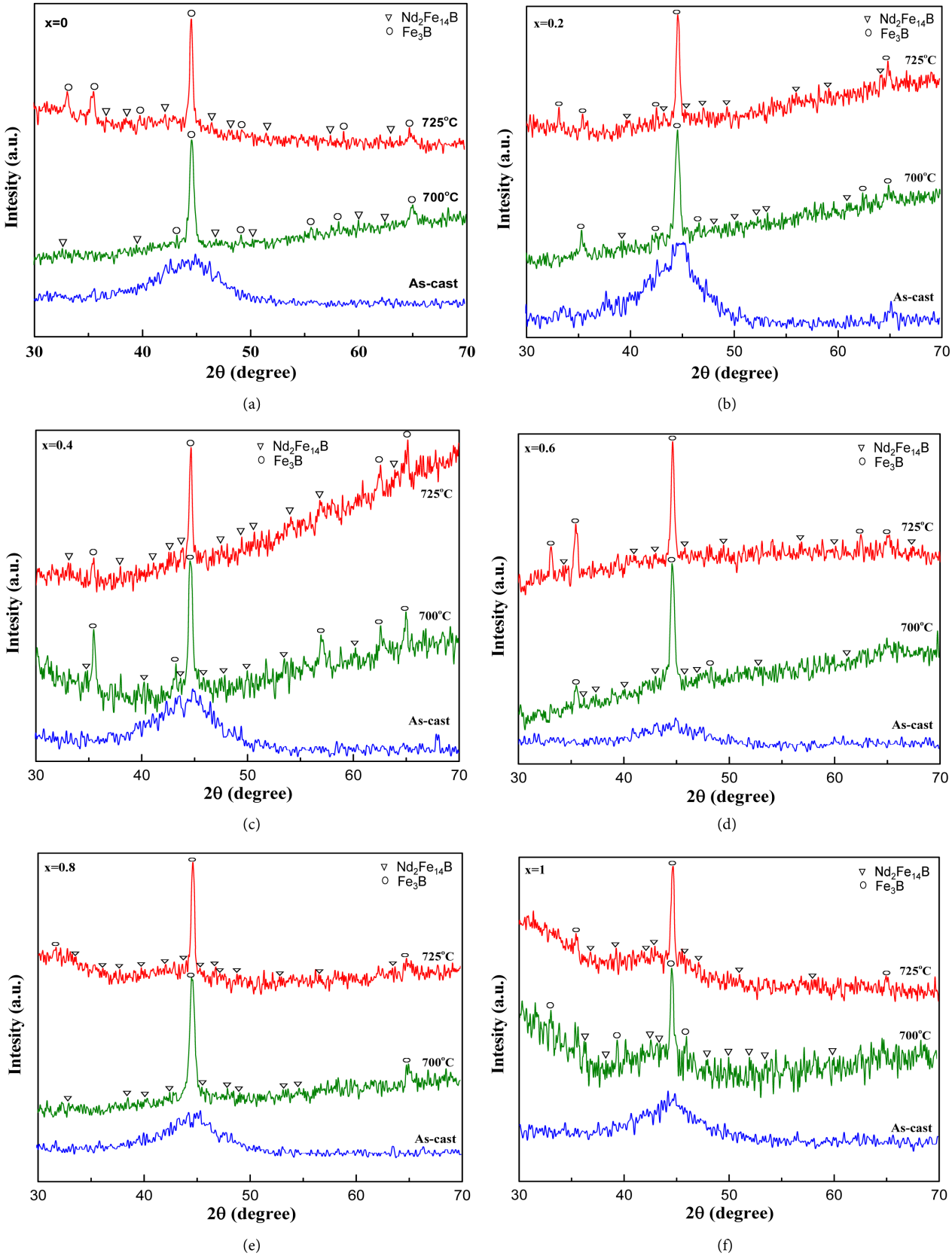


**Figure 2.** X-ray diffraction pattern of $Nd_{4-x}Tb_xFe_{83.5}Co_5Cu_{0.5}Nb_1B_6$ (x = 0, 0.2, 0.4, 0.6, 0.8 and 1) samples in the as-cast and annealed at various temperatures for 10 min.

ribbons are in fully amorphous state in the as-cast condition. Hard magnetic phase ($Nd_2Fe_{14}B$) has formed in small amount in association with the soft phase ($Fe_3B$) for the annealing temperature of 700˚C. At higher annealing temperature of 725˚C, the diffraction patterns for the mixture of soft and hard phases are more clear [8].

The diffraction peaks around 33˚ and 65˚ due to $Fe_3B$ and $Nd_2Fe_{14}B$ start to appear from 700˚C. The intensity of the diffraction peaks around 45˚ due to $Fe_3B$ increases significantly at 700˚C and 725˚C. For the composition of $Nd_{4-x}Tb_xFe_{83.5}Co_5Cu_{0.5}Nb_1B_6$ (x = 0), the peaks around 36˚ - 43˚ and at 48˚ - 65˚ due to $Nd_2Fe_{14}B$ also grow up in the ribbon at 700˚C. From the above results, it can be said that soft phase and hard phase both exist collectively at 700˚C. The diffraction peaks around 33˚ - 36˚ due to $Fe_3B$ are well formed and besides the diffraction peaks around 36˚ - 43˚ and at 47˚ - 65˚ due to $Nd_2Fe_{14}B$ and $Fe_3B$ are exist collectively at 725˚C as shown in **Figure 2(a)**. The diffraction patterns are shown in **Figure 2(b)** for the composition of x = 0.2. Around 34˚ - 65˚, the diffraction peaks due to $Fe_3B$ and $Nd_2Fe_{14}B$ start to appear from 700˚C [9]. The peak due to $Fe_3B$ at 35˚ is well formed and clearer at 700˚C and some peaks for soft phase are well formed around 33˚ - 35˚ at 725˚C. The diffraction peaks around 36˚ - 43˚ and at 47˚ - 65˚ due to $Nd_2Fe_{14}B$ also grown up in the ribbon with the increase in temperature. From the above results, it can be said that $Fe_3B$ and $Nd_2Fe_{14}B$ start to be crystallized collectively at 700˚C. We have also found that at higher annealing temperature of 725˚C characteristic patterns of the mixture of soft and hard phases. The maximum intensity of the diffraction peak has been found at 700˚C. Similar phases are growing for other compositions in the closer range of temperature. The analysis of Mössbauer spectra was carried out based on these experimental results.

The Mössbauer spectra of nanocomposite melt spun ribbon samples of compositions $Nd_{4-x}Tb_xFe_{83.5}Co_5Cu_{0.5}Nb_1B_6$ (x = 0, 0.2, 0.4, 0.6, 0.8 and 1) for as-cast and annealed samples at two different temperatures like 712˚C and 725˚C are shown in **Figure 3**. We have seen experimental and theoretical data were well fitted during Mössbauer analysis. The Mössbauer spectrum of the as-cast and annealed condition for all composition shows sextet pattern and these sextet patterns confirms that the materials shows ferromagnetic properties. The spectra consist of broad, overlapped lines assigned to disordered structural positions of resonant atoms and the sharp narrow lines indicate a presence of BCC-Fe crystallites. The corresponding hyperfine parameters for all the compositions in the as-cast and annealed condition are shown in **Table 1(a)** and **Table 1(b)**. The parameters H, dH and $V_o$ are represents hyperfine field, hyperfine field distribution for full width half maximum (FWHM) and isomer shift respectively. In the case of the alloy of these compositions annealed at 712˚C and 725˚C several sextets corresponding to $Nd_2Fe_{14}B$ and $Fe_3B$ were supposed. In the analysis of the Mössbauer spectra of the alloys, the contribution of $Nd_2Fe_{14}B$ and $Fe_3B$ to the spectra was taken into account with the following assumptions. The relative intensity ratios of the sextets were assumed to be 3:2:1:1:2:3, that is, a random

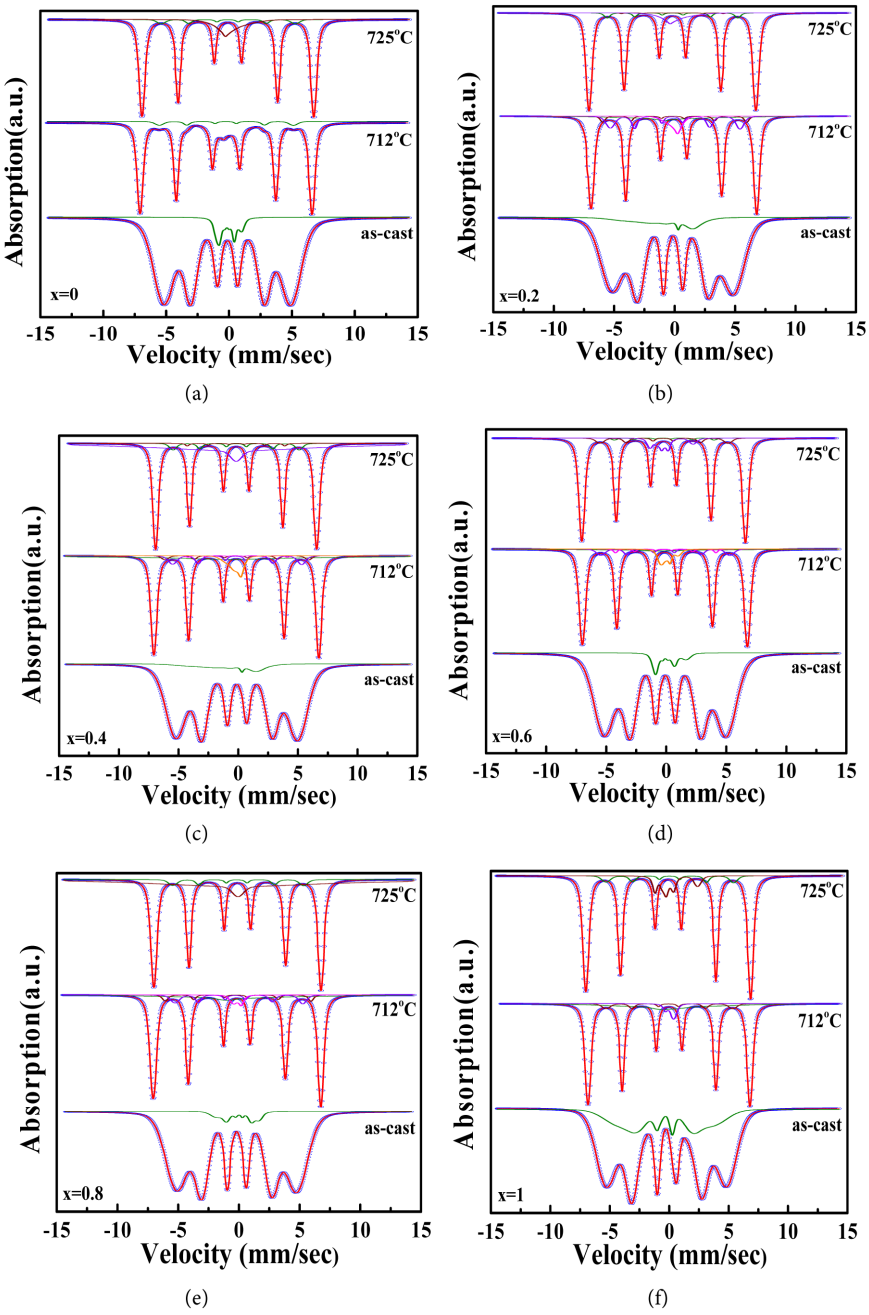


**Figure 3.** The Mössbauer spectra of $Nd_{4-x}Tb_xFe_{83.5}Co_5Cu_{0.5}Nb_1B_6$ (x = 0, 0.2, 0.4, 0.6, 0.8 and 1) in the as-cast and annealed at different temperatures for 10 min.

orientation of nanocrystalline grains. The widths of all sextets were considered the approximately same as shown in **Figure 3** [9]. X-ray diffraction and differential scanning calorimetry measurements suggested that the amorphous sextet should be assigned to an amorphous phase [9]. We have seen here $Fe_3B$ species were increased with the increase of annealing temperature and $Nd_2Fe_{14}B$ species were decreased with the increase of annealing temperature for all the ribbon samples. The weight fraction of phases of $Nd_2Fe_{14}B/Fe_3B$ in the alloys is approximately higher at 712˚C.

**Table 1.** (a). Hyperfine parameters for Mössbauer spectra of $Nd_{4-x}Tb_xFe_{83.5}Co_5Cu_{0.5}Nb_1B_6$ (x = 0, 0.2 and 0.4) in the as-cast and annealed conditio; (b). Hyperfine parameters for Mössbauer spectra of $Nd_{4-x}Tb_xFe_{83.5}Co_5Cu_{0.5}Nb_1B_6$ (x = 0.6, 0.8 and 1) in the as-cast and annealed condition.

(a)

| $Tb_x$ | Anneal condition | Phase | H (kG) | dH | $V_o$ (mm/s) | Rel. Area | Total wt. of phases | Wt. fraction of Phases |
|---|---|---|---|---|---|---|---|---|
| x = 0 | As-cast | Am | 50.27 | 0.1 | 0 | 0.062 | 1.07 | Amorphous |
| | | | 249.75 | 0.538 | 0 | 1.008 | | |
| | 712˚C | $A_1$ | 18.82 | 0.1 | 0.546 | 0.05 | 1.03 | $A_1$~0.05 |
| | | $Fe_3B$ | 138.48 | 0.01 | 0.124 | 0.71 | | $Fe_3B$~0.710 |
| | | $Nd_2Fe_{14}B$ | 308.55 | 0.795 | 0.115 | 0.27 | | $Nd_2Fe_{14}B$~0.270 |
| | 725˚C | $A_1$ | 20.7 | 0.971 | 0.23 | 0.1 | 1.07 | $A_1$~0.10 |
| | | $Fe_3B$ | 119.81 | 0.01 | 0.593 | 0.08 | | $Fe_3B$~0.720 |
| | | $Fe_3B$ | 264.6 | 0.2 | 0.392 | 0.64 | | $Nd_2Fe_{14}B$~0.250 |
| | | $Nd_2Fe_{14}B$ | 335.6 | 0.164 | 0.474 | 0.25 | | |
| x = 0.2 | As-cast | Am | 135.09 | 0.945 | 0 | 0.06 | 1.01 | Amorphous |
| | | | 245.49 | 0.653 | 0 | 0.94 | | |
| | 712˚C | $A_1$ | 14.7 | 0.46 | 0.043 | 0.05 | 1.07 | $A_1$~0.05 |
| | | $Fe_3B$ | 147.15 | 4.681 | 0 | 0.09 | | $Fe_3B$~0.844 |
| | | $Fe_3B$ | 264.6 | 0.2 | 0 | 0.754 | | $Nd_2Fe_{14}B$~0.183 |
| | | $Nd_2Fe_{14}B$ | 294 | 0.064 | 0.014 | 0.08 | | |
| | | $Nd_2Fe_{14}B$ | 338.1 | 0.121 | 0.014 | 0.103 | | |
| | 725˚C | $A_1$ | 25.73 | 10 | 0.133 | 0.1 | 1.07 | $A_1$~0.10 |
| | | $Fe_3B$ | 137.89 | 0.01 | 0.145 | 0.04 | | $Fe_3B$~0.86 |
| | | $Fe_3B$ | 264.6 | 0.06 | 0.428 | 0.82 | | $Nd_2Fe_{14}B$~0.11 |
| | | $Nd_2Fe_{14}B$ | 294 | 0.08 | 0.6 | 0.06 | | |
| | | $Nd_2Fe_{14}B$ | 338.1 | 0.18 | 0.6 | 0.05 | | |
| x = 0.4 | As-cast | Am | 34.99 | 0.1 | 0.189 | 0.04 | 1.02 | Amorphous |
| | | | 251.22 | 0.552 | 0 | 0.98 | | |
| | 712˚C | $A_1$ | 14.7 | 0.46 | 0.043 | 0.05 | 1.07 | $A_1$~0.05 |
| | | $Fe_3B$ | 147.15 | 4.681 | 0 | 0.08 | | $Fe_3B$~0.838 |
| | | $Fe_3B$ | 203.3 | 0.01 | 0.014 | 0.008 | | $Nd_2Fe_{14}B$~0.182 |
| | | $Fe_3B$ | 264.6 | 0.2 | 0 | 0.75 | | |
| | | $Nd_2Fe_{14}B$ | 294 | 0.064 | 0.014 | 0.08 | | |
| | | $Nd_2Fe_{14}B$ | 338.1 | 0.121 | 0.014 | 0.102 | | |
| | 725˚C | $A_1$ | 25.73 | 10 | 0.133 | 0.1 | 1.05 | $A_1$~0.10 |
| | | $Fe_3B$ | 119.11 | 0.01 | 0.145 | 0.03 | | $Fe_3B$~0.85 |
| | | $Fe_3B$ | 204.6 | 0.163 | 0.016 | 0.82 | | $Nd_2Fe_{14}B$~0.10 |
| | | $Nd_2Fe_{14}B$ | 294 | 0.08 | 0.6 | 0.05 | | |
| | | $Nd_2Fe_{14}B$ | 337.95 | 0.117 | 0.016 | 0.05 | | |

$A_1$-remaining amorphous phase.

(a)

| $Tb_x$ | Anneal condition | Phase | H (kG) | dH | $V_o$ (mm/s) | Rel. Area | Total wt. of phases | Wt. fraction of Phases |
|---|---|---|---|---|---|---|---|---|
| x = 0.6 | As-cast | Am | 65.71 | 0.192 | 0 | 0.04 | 1.03 | Amorphous |
| | | | 250.78 | 0.585 | 0 | 0.99 | | |
| | 712˚C | $A_1$ | 34.55 | 0.165 | 0.287 | 0.065 | 1.04 | $A_1$~0.065 |
| | | $Fe_3B$ | 205.8 | 0.01 | 0 | 0.022 | | $Fe_3B$~0.824 |
| | | $Fe_3B$ | 264.6 | 0.2 | 0 | 0.802 | | $Nd_2Fe_{14}B$~0.151 |
| | | $Nd_2Fe_{14}B$ | 294 | 0.064 | 0.014 | 0.048 | | |
| | | $Nd_2Fe_{14}B$ | 338.1 | 0.121 | 0.014 | 0.103 | | |

**Continued**

| | | | | | | | |
|---|---|---|---|---|---|---|---|
| | | $A_1$ | 65.12 | 0.171 | 0.315 | 0.07 | |
| | | $Fe_3B$ | 206.39 | 0.1 | 0.004 | 0.015 | $A_1$~0.07 |
| | 725˚C | $Fe_3B$ | 264.6 | 0.2 | 0.428 | 0.822 | 1.02 $Fe_3B$~0.837 |
| | | $Nd_2Fe_{14}B$ | 294 | 0.08 | 0.6 | 0.06 | $Nd_2Fe_{14}B$~0.113 |
| | | $Nd_2Fe_{14}B$ | 338.1 | 0.123 | 0.004 | 0.053 | |
| x = 0.8 | As-cast | Am | 87.47 | 0.254 | 0.338 | 0.045 | 1.03 Amorphous |
| | | | 245.2 | 0.645 | 0 | 0.985 | |
| | | $A_1$ | 23.96 | 0.1 | 0.079 | 0.03 | |
| | | $Fe_3B$ | 204.77 | 5.9 | 0.059 | 0.075 | $A_1$~0.03 |
| | 712˚C | $Fe_3B$ | 257.69 | 0.2 | 0.059 | 0.766 | 1.01 $Fe_3B$~0.841 |
| | | $Nd_2Fe_{14}B$ | 294 | 0.091 | 0.014 | 0.036 | $Nd_2Fe_{14}B$~0.139 |
| | | $Nd_2Fe_{14}B$ | 338.1 | 0.13 | 0.059 | 0.103 | |
| | | $A_1$ | 14.7 | 0.1 | 0.145 | 0.041 | |
| | | $Fe_3B$ | 207.42 | 3.378 | 0 | 0.025 | $A_1$~0.041 |
| | 725˚C | $Fe_3B$ | 264.6 | 0.2 | 0 | 0.85 | 1.03 $Fe_3B$~0.875 |
| | | $Nd_2Fe_{14}B$ | 294 | 0.08 | 0.6 | 0.06 | $Nd_2Fe_{14}B$~0.114 |
| | | $Nd_2Fe_{14}B$ | 338.1 | 0.123 | 0 | 0.054 | |
| x = 1 | As-cast | Am | 193.9 | 0.904 | 0 | 0.256 | 1.04 Amorphous |
| | | | 251.81 | 0.569 | 0 | 0.784 | |
| | | $A_1$ | 14.7 | 0.46 | 0.043 | 0.05 | |
| | | $Fe_3B$ | 115.69 | 10 | 0.492 | 0.051 | $A_1$~0.05 |
| | 712˚C | $Fe_3B$ | 264.6 | 0.2 | 0.016 | 0.747 | 1.03 $Fe_3B$~0.798 |
| | | $Nd_2Fe_{14}B$ | 294 | 0.064 | 0.014 | 0.08 | $Nd_2Fe_{14}B$~0.182 |
| | | $Nd_2Fe_{14}B$ | 338.1 | 0.122 | 0.017 | 0.102 | |
| | | $A_1$ | 65.86 | 10 | 0.139 | 0.09 | $A_1$~0.09 |
| | | $Fe_3B$ | 119.11 | 0.01 | 0.145 | 0.03 | $Fe_3B$~0.854 |
| | 725˚C | $Fe_3B$ | 261.66 | 0.2 | 0.434 | 0.824 | 1.05 $Nd_2Fe_{14}B$~0.106 |
| | | $Nd_2Fe_{14}B$ | 294 | 0.07 | 0.6 | 0.056 | |
| | | $Nd_2Fe_{14}B$ | 338.1 | 0.115 | 0.434 | 0.05 | |

$A_1$-remaining amorphous phase.

When the Tb concentration is zero, weight fraction of both the phases increased with the increase of annealing temperature and for higher Tb concentration (x = 0.8 and 1), the materials shows higher value of weight fraction at 725˚C as shown in Table 1. The symbols Am and $A_1$ represents amorphous phase and remaining amorphous phase respectively. We have found that the remaining amorphous phase increased due to the increase of annealing temperature for all compositions. It can be said that substitution element Tb influence the value of hyperfine field and increase in annealing temperature induces formation of higher volume fraction of the crystalline phase. Higher hyperfine field for these alloys indicate the presence of regions inside the amorphous residual matrix where Fe atoms are having higher magnetic moments [10].

We have investigated the temperature dependence of magnetization results for the ribbon samples were presented in Figure 4, where the applied magnetic field was 10 kG. Two magnetic phases which are the hard phase and soft phase for all the ribbon samples have been identified. We have found two magnetic transitions (Curie point) for as-cast and annealed samples of the composition x = 0. For the as-cast sample, the first transition is around 330˚C and it corresponds to the $Nd_2Fe_{14}B$ phase while for the annealing temperatures of 675˚C, 712˚C and 725˚C, these transitions are around 340˚C, 345˚C and 350˚C corresponding to the $Nd_2Fe_{14}B$ phase respectively. The second transition is around

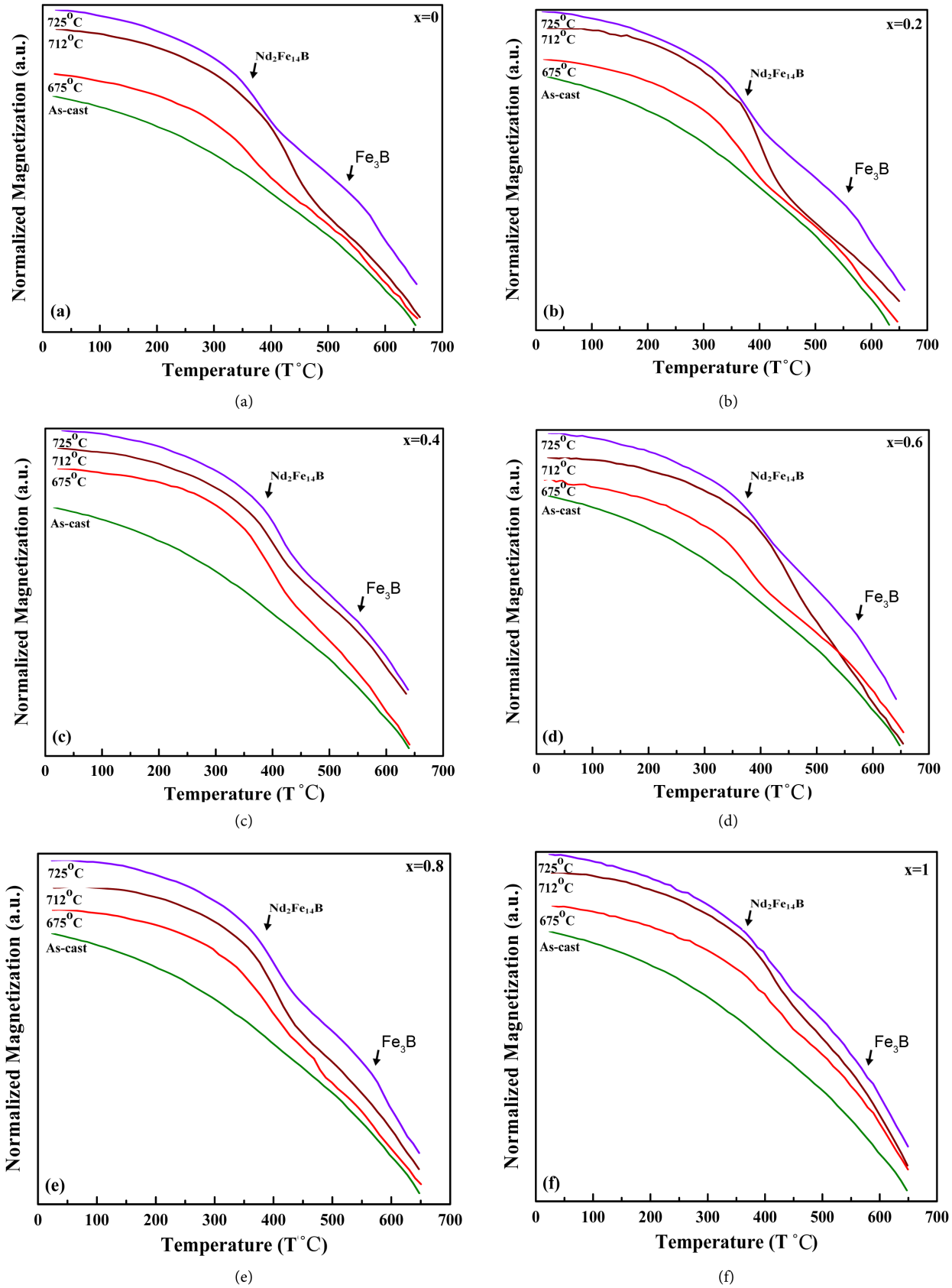


**Figure 4.** Temperature dependence of the magnetization for $Nd_{4-x}Tb_xFe_{83.5}Co_5Cu_{0.5}Nb_1B_6$ (x = 0, 0.2, 0.4, 0.6, 0.8 and 1) samples in the as-cast and annealed condition.

520˚C for as-cast sample and it corresponds to the $Fe_3B$ phase while for the annealed samples, the transitions are around 540˚C, 560˚C and 570˚C corresponding to the $Fe_3B$ phase as shown in **Figure 4(a)**. For the composition of x = 0.2, the first transition is around 320˚C and it corresponds to the $Nd_2Fe_{14}B$ phase, while for the annealed at 675˚C, 712˚C and 725˚C samples these transitions are around 330˚C, 340˚C and 350˚C corresponding to the $Nd_2Fe_{14}B$ phase respectively. The second transition is around 500˚C for as-cast sample and it corresponds to the $Fe_3B$ phase, while for the annealed samples these transitions are around 550˚C, 510˚C and 580˚C corresponding to the $Fe_3B$ phase as shown in **Figure 4(b)**. In the case of x = 0.4 samples, the first transition is around 330˚C for as-cast sample and it corresponds to the $Nd_2Fe_{14}B$ phase, while for the annealed at 675˚C, 712˚C and 725˚C these transitions are around 360˚C, 370˚C and 380˚C corresponding to the $Nd_2Fe_{14}B$ phase respectively. The second transition is around 500˚C for as-cast sample and it corresponds to the $Fe_3B$ phase while for the annealed samples, these transitions are around 510˚C, 540˚C and 560˚C corresponding to the $Fe_3B$ phase as shown in **Figure 4(c)**. For the composition of x = 0.6, the first transition is around 320˚C for as-cast and 350˚C, 370˚C and 380˚C for annealed samples corresponding to the hard phase. The second transition temperatures are 500˚C for the as-cast and 550˚C, 540˚C and 560˚C for the annealed samples corresponding to the soft phase as shown in **Figure 4(d)**. Similarly we have seen for the composition of x = 0.8, the first transition temperatures are around 330˚C for as-cast and 340˚C, 350˚C and 360˚C for the annealed samples corresponding to the $Nd_2Fe_{14}B$ phase and second transition is around 520˚C for as-cast and 560˚C, 570˚C and 580˚C for the annealed sample corresponding to the $Fe_3B$ phase as shown in **Figure 4(e)**.

The first transition is at 320˚C and it corresponds to the $Nd_2Fe_{14}B$ phase while for the annealed at 675˚C, 712˚C and 725˚C samples these transitions are around 350˚C, 360˚C and 370˚C corresponding to the $Nd_2Fe_{14}B$ phase respectively. The second transition is around 500˚C for as-cast sample and it corresponds to the $Fe_3B$ phase, while for the annealed samples this transition is around 550˚C, 560˚C and 570˚C corresponding to the $Fe_3B$ phase in the case of x = 1 as shown in **Figure 4(f)** [11]. From the above results, it can be stated that the samples of every composition shows two transition temperatures clearly and first transition temperature is formed due to the hard phase and second transition temperature due to the soft phase. We have determined Curie temperature ($T_c$) from dM/dT versus temperature analysis with the help of temperature dependence of magnetization measurement by using vibrating sample magnetometer. In the case of as-cast and annealed x = 0 samples two magnetic (Curie point) transitions were formed.

For the as-cast sample, the Curie temperature ($T_{c1}$) due to first transition is 340˚C and it corresponds to the $Nd_2Fe_{14}B$ phase while for the annealing temperatures of 675˚C, 712˚C, and 725˚C, the Curie temperatures are 350˚C, 360˚C and 380˚C corresponding to the $Nd_2Fe_{14}B$ phase respectively. The Curie temperature ($T_{c2}$) due to second transition is 520˚C for as-cast sample and it corresponds to

the $Fe_3B$ phase while for the annealed samples, Curie temperatures for second transitions are 530˚C, 540˚C and 540˚C corresponding to the $Fe_3B$ phase. Similarly Curie temperatures for other compositions have been determined and it can be stated that the Curie temperature increases with the increase of annealing temperature which are shown in Table 2.

For the nanocomposite melt spun ribbon samples of composition $Nd_{4-x}Tb_xFe_{83.5}Co_5Cu_{0.5}Nb_1B_6$ (x = 0, 0.2, 0.4, 0.6, 0.8 and 1), hysteresis parameters have been determined in as-cast condition and annealed at different crystallization temperatures by hysteresis loop analysis are shown in Figure 5. Saturation

Table 2. Curie temperature for the samples of $Nd_{4-x}Tb_xFe_{83.5}Co_5Cu_{0.5}Nb_1B_6$ (x = 0, 0.2, 0.4, 0.6, 0.8 and 1) in the as-cast and annealed at various temperatures with annealing time 10 min.

| $Tb_x$ | Annealing condition | $Tc_1$ (˚C) | $Tc_2$ (˚C) |
|---|---|---|---|
| x = 0 | As-cast | 340 | 520 |
| | 675˚C | 350 | 530 |
| | 712˚C | 360 | 540 |
| | 725˚C | 380 | 540 |
| x = 0.2 | As-cast | 340 | 520 |
| | 675˚C | 380 | 520 |
| | 712˚C | 400 | 540 |
| | 725˚C | 400 | 550 |
| x = 0.4 | As-cast | 340 | 530 |
| | 675˚C | 370 | 540 |
| | 712˚C | 400 | 540 |
| | 725˚C | 420 | 560 |
| x = 0.6 | As-cast | 340 | 530 |
| | 675˚C | 360 | 530 |
| | 712˚C | 390 | 540 |
| | 725˚C | 400 | 580 |
| x = 0.8 | As-cast | 340 | 540 |
| | 675˚C | 360 | 540 |
| | 712˚C | 380 | 560 |
| | 725˚C | 400 | 580 |
| x = 1 | As-cast | 340 | 540 |
| | 675˚C | 370 | 550 |
| | 712˚C | 410 | 560 |
| | 725˚C | 410 | 560 |

magnetization, coercivity, remanent ratio and maximum energy product were obtained from the hysteresis loops as shown in Table 3. We have found that, the

Table 3. Hysteresis loop parameters for the samples of $Nd_{4-x}Tb_xFe_{83.5}Co_5Cu_{0.5}Nb_1B_6$ (x = 0, 0.2, 0.4, 0.6, 0.8 and 1) annealed at various temperatures and for annealing time 10 min [12].

| $Tb_x$ | Annealing temperature (˚C) | $M_s$ (emu/g) | $H_c$ (KOe) | $M_r/M_s$ | $(BH)_{max}$ (MGOe) |
|---|---|---|---|---|---|
| x = 0 | 675 | 141.3 | 0.99 | 0.42 | 0.82 |
| | 687 | 149.5 | 1.05 | 0.48 | 1.13 |
| | 700 | 190.8 | 1.06 | 0.61 | 2.55 |
| | 712 | 136.1 | 0.58 | 0.33 | 0.00 |
| | 725 | 173.3 | 0.18 | 0.25 | 0.00 |
| x = 0.2 | 675 | 142.1 | 0.96 | 0.35 | 0.38 |
| | 687 | 134.3 | 1.50 | 0.47 | 1.25 |
| | 700 | 156.5 | 2.24 | 0.63 | 4.84 |
| | 712 | 151 | 1.90 | 0.65 | 4.14 |
| | 725 | 152.4 | 0.24 | 0.36 | 0.00 |
| x = 0.4 | 675 | 129.4 | 1.06 | 0.42 | 0.88 |
| | 687 | 140.6 | 1.54 | 0.57 | 2.18 |
| | 700 | 211.4 | 1.34 | 0.49 | 2.43 |
| | 712 | 124.7 | 1.09 | 0.47 | 0.91 |
| | 725 | 151.5 | 0.56 | 0.37 | 0.41 |
| x = 0.6 | 675 | 150.6 | 1.29 | 0.55 | 2.07 |
| | 687 | 146.3 | 0.82 | 0.44 | 0.62 |
| | 700 | 180.9 | 1.35 | 0.55 | 2.23 |
| | 712 | 151.4 | 0.89 | 0.46 | 1.01 |
| | 725 | 157.9 | 0.29 | 0.29 | 0.00 |
| x = 0.8 | 675 | 147.7 | 1.59 | 0.46 | 1.81 |
| | 687 | 135.7 | 1.71 | 0.58 | 2.33 |
| | 700 | 176.9 | 2.36 | 0.66 | 6.11 |
| | 712 | 93.3 | 1.35 | 0.43 | 0.80 |
| | 725 | 141.2 | 0.62 | 0.34 | 0.45 |
| x = 1 | 675 | 166.3 | 0.63 | 0.49 | 1.12 |
| | 687 | 142.4 | 0.57 | 0.47 | 0.08 |
| | 700 | 204.4 | 0.77 | 0.53 | 1.49 |
| | 712 | 179.5 | 0.51 | 0.38 | 0.61 |
| | 725 | 165.8 | 0.40 | 0.36 | 0.17 |

coercivity increase with the increase of annealing temperature, remain almost higher at 700˚C and then decrease while varying the higher annealing temperature. For the composition of x = 0.8, the highest value of coercivity ($H_c$) has been obtained at optimal annealing temperature 700˚C. We have observed for all the compositions the maximum energy product $(BH)_{max}$ increase with the increase of annealing temperature, remain almost higher at optimal annealing temperature 700˚C and then decrease while varying the annealing temperature. The highest value of maximum energy product has been achieved for the composition of x = 0.8 at 700˚C. As shown in **Table 3** and **Figure 5** saturation magnetization ($M_s$) increases initially with the increase of annealing temperature, shows highest value at 700˚C and then decreases drastically with the increase of annealing temperature. The highest value of $M_s$ has been achieved for the composition of x = 0.4. We have seen that addition of Tb and there is some fluctuation in the variation of magnetization with the increase of annealing temperature.

This is probably because the optimum crystallization temperature was in between the annealing temperatures presented in this study. However, $M_r/M_s$ ratio remains almost constant for most of the annealing temperature other than 725˚C which is over-annealed temperature for most of the samples. According to the previous results reported [12], the effect of annealing process for this kind of material is important to enhance $H_c$ and $(BH)_{max}$. In order to enhance the hard magnetic property, the nanocomposite ribbons were annealed at various temperatures 675˚C, 687˚C, 700˚C, 712˚C and 725˚C for 10 min. The variation of the $H_c$, $M_r/M_s$ and $(BH)_{max}$ with the annealing temperatures are shown in **Figure 6**. Since the magnetic properties of various compositions are sensitive to the annealing temperature, it is therefore essential that individual annealing conditions should be adopted for the particular alloy composition [13]. We have observed that after annealing, shape of the hysteresis loops is strongly changed with annealing temperature and concentration of Tb. The hysteresis loops of all the ribbons are greatly expanded at most of the selected annealing temperatures. That means the hard magnetic phases were formed in the annealed alloys resulting in an increase in coercivity of the materials [14]. The coercivity increases with the increase of Tb concentration as shown in **Figure 5**. From **Figure 6(a)**, the coercivity of the alloy is only 1.06 kOe for Tb concentration (x = 0), but when Tb concentration is increased by x = 0.2, the coercivity is enhanced by 2.24 kOe at the optimal annealing temperature 700˚C. In comparison with that of the x = 0 sample the coercivity of the sample with x = 0.2 is increased by an amount larger than 110%. It is interesting to find that, with different concentrations of Tb, the ribbons have the same annealing temperature of 700˚C to achieve the highest coercivity.

The highest value of $H_c$ is 2.36 kOe obtained on the sample with x = 0.8 at optimal annealing temperature 700˚C [15]. The remanent ratio, $M_r/M_s$ for x = 0 is also found 0.61. When Tb concentration is increased from x = 0 to 1%, the $M_r/M_s$ reduced more than 13% [16]. At optimal annealing temperature 700˚C, the $M_r/M_s$ value is 0.49 for x = 0.4 at % as shown in **Figure 6(b)**. The maximum energy product $(BH)_{max}$ also increases with the increase of Tb concentration. The

largest value of $(BH)_{max}$ is 6.11 MGOe achieved on the sample with Tb concentration of 0.8 at % where the value of $(BH)_{max}$ is 2.55 MGOe for the sample without Tb concentration at optimal annealing temperature 700˚C as shown in **Figure 6(c)**. At the annealing temperature of 700˚C, the coercivity, maximum

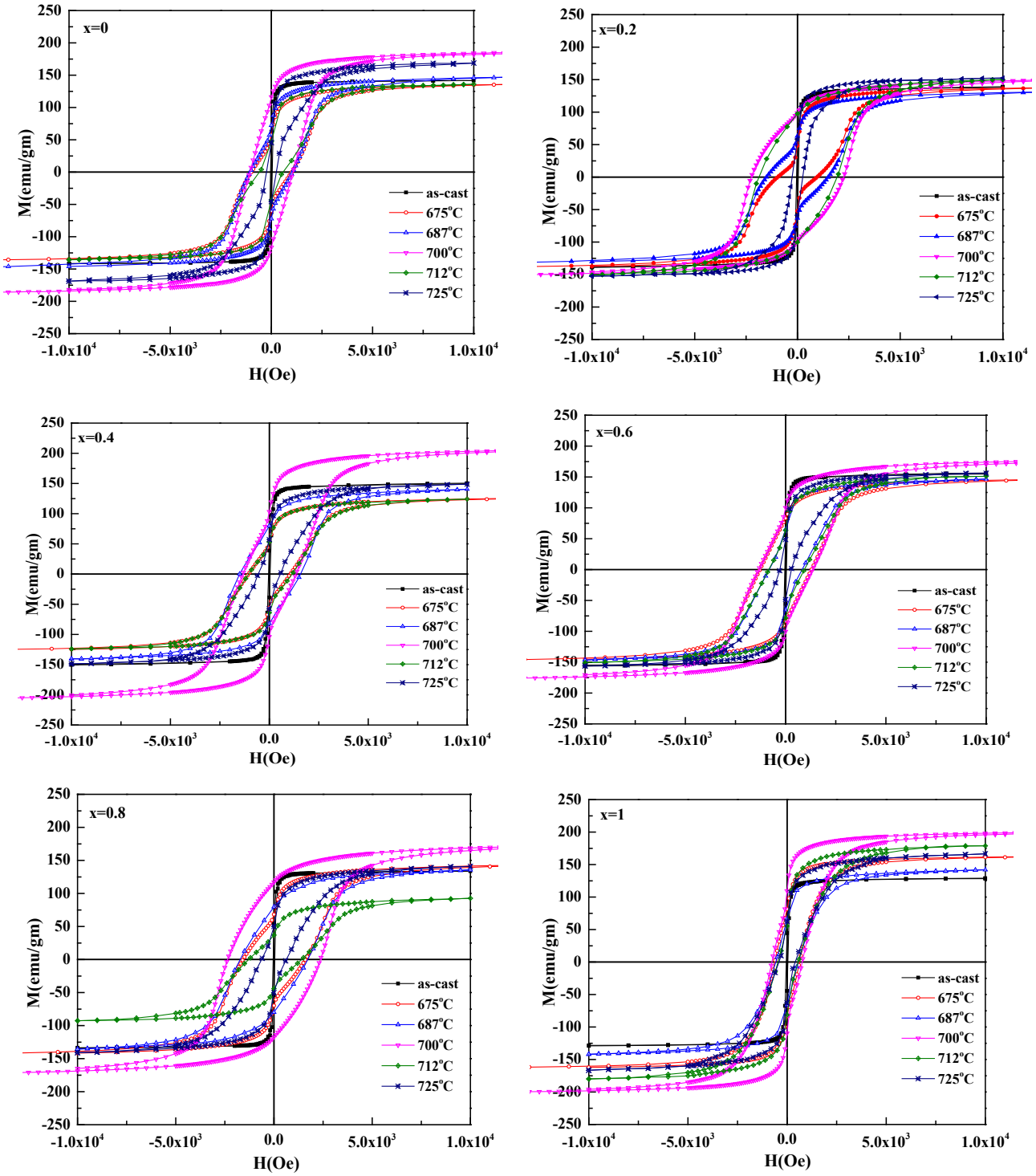


**Figure 5.** Hysteresis loops of $Nd_{4-x}Tb_xFe_{83.5}Co_5Cu_{0.5}Nb_1B_6$ (x = 0, 0.2, 0.4, 0.6, 0.8 and 1) sample in the as-cast and annealed at different temperatures for 10 min.

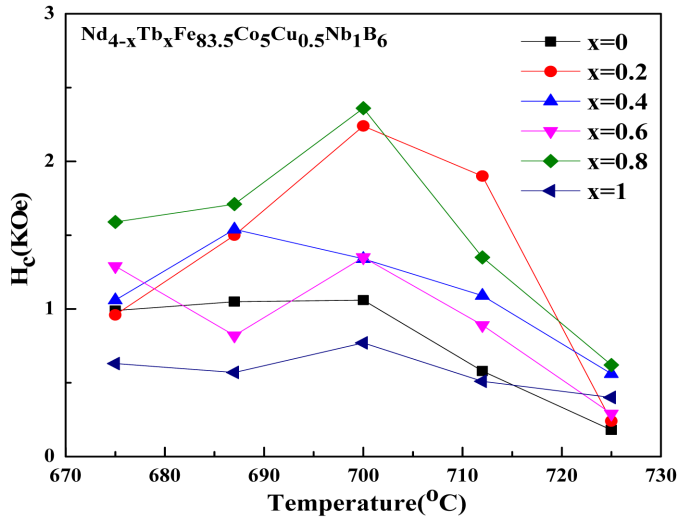


(a)

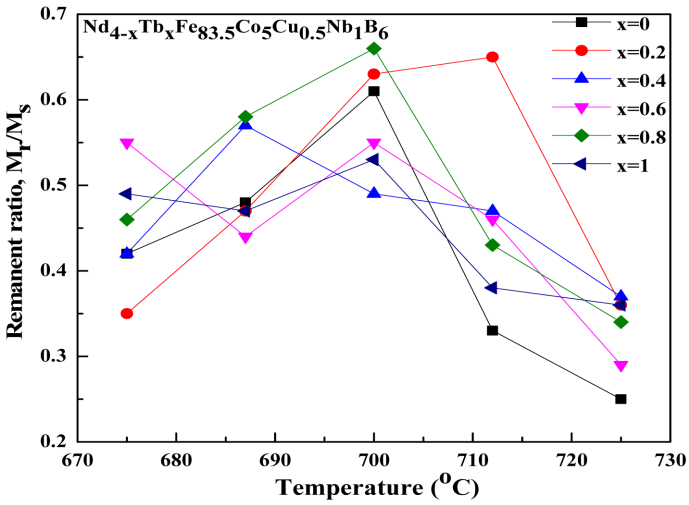


(b)

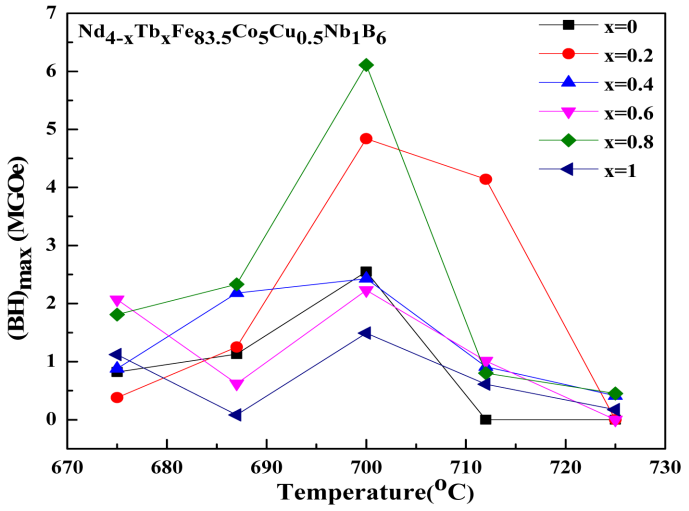


(c)

**Figure 6.** (a) Coercivity ($H_c$), (b) remanent ratio ($M_r/M_s$), and (c) maximum energy product $(BH)_{max}$ versus annealing temperature of $Nd_{4-x}Tb_xFe_{83.5}Co_5Cu_{0.5}Nb_1B_6$ alloys.

energy product and remanent ratio of x = 0 are 1.06 kOe, 2.55 MGOe and 0.61 respectively, while the coercivity, maximum energy product and remanent ratio of x = 0.8 are 2.36 kOe, 6.11 MGOe and 0.66. From these results it can be stated that higher coercivity, maximum energy product and reduced remanent ratio have been achieved for all the compositions. Though an enhancement of coercivity takes place due to the higher anisotropy field when Nd is partially substituted by Tb and remanent ratio is decreased due to antiferromagnetic coupling between rare earth and transition metal [17] [18] [19].

## 4. Conclusions

Tb substituted amorphous ribbons of composition $Nd_{4-x}Tb_xFe_{83.5}Co_5Cu_{0.5}Nb_1B_6$ (x = 0, 0.2, 0.4, 0.6, 0.8 and 1) have been studied to observe the exchange coupled soft and hard magnetic phases in the nanocrystalline state. According to the crystallization temperatures DSC traces, the nanocomposite samples have been annealed at 675˚C, 687˚C, 700˚C, 712˚C and 725˚C for 10 min. The samples were characterized by XRD with $CuK_a$ radiation and we have seen soft and hard phases are formed due to the samples annealed at crystallization temperatures. The weight fractions of both the phases $Fe_3B$ and $Nd_2Fe_{14}B$ in crystallization process were estimated by Mössbauer spectroscopy analysis. A practically amorphous alloy as quenched starts to crystallize at 675˚C in the vacuum annealing process, but the crystallized grains are too fine to be observed with the XRD method and Mössbauer spectroscopy. Co-rich and Tb substitution has significantly enhanced the value of coercivity ($H_c$) and maximum energy product $(BH)_{max}$. For the sample of composition x = 0.8 the highest values of coercivity ($H_c$) 2.36 kOe has been achieved. At the optimal annealing temperature 700˚C, the maximum energy product $(BH)_{max}$ has been found to be 6.11 MGOe for the composition of x = 0.8. We have observed enhancement of exchange coupling between soft and hard phases causes a highly reduced remanent ratio ($M_r/M_s$) up to 0.49 at optimal annealing temperature 700˚C. Temperature dependence of magnetization analysis gives transition region where the soft and hard phases were formed. We have determined Curie temperature ($T_c$) for as-cast and annealed samples with the help of temperature dependence of magnetization measurement. Curie temperature increases with the increase of annealing temperature. In our experiment, we were able to enhance both $H_c$ and $(BH)_{max}$ for most of the compositions than the high anisotropic Tb containing exchange spring ribbons. The optimal annealing conditions for the best hard magnetic performance of the ribbons were obtained. The composition dependence of the structure and magnetic properties of the alloys were discussed.

## Acknowledgements

The authors acknowledge respectfully to Ministry of Science and Technology, Government of the People's Republic of Bangladesh and highly acknowledge the support provided by Materials Science Division, Atomic Energy Centre, Dhaka, Bangladesh. Financial support provided by the International Program for Physi-

cal Sciences, Uppsala University, Sweden is acknowledged. The authors acknowledge kind help provided by Prof. N. Q. Liem, Director, Institute of Materials Science, Vietnam Academy of Science and Technology, Hanoi, Vietnam and department of Physics, Jahangirnagar University, Savar, Dhaka, Bangladesh.

## References

[1] Coehoorn, R., de Mooij, D.B., Duchateau, J.P.W.B. and Buchow, K.H.J. (1998) Novel Permanent Magnetic Materials Made by Rapid Quenching. *Journal de Physique*, **49**, 669-670.

[2] Kneller, E.F. and Hawig, R. (1991) The Exchange-Spring Magnet: A New Material Principle for Permanent Magnets. *IEEE Transactions on Magnetics*, **27**, 3588-3600. https://doi.org/10.1109/20.102931

[3] Miyoshi, T., Kanekiyo, H. and Hirosawa, S. (2005) Effects of Nb Addition on Structural and Magnetic Properties of Fe-B/Nd/sub 2/Fe/sub 14/B-Based Nanocomposite Magnets. *IEEE Transactions on Magnetics*, **41**, 3865-3867. https://doi.org/10.1109/TMAG.2005.854949

[4] Villas-Boas, V., Missell, F.P. and da Cunha, S.F. (1998) Magnetic Properties of $La_2(Fe_{1-x}Co_x)_{14}B$ and $Nd_2(Fe_{1-x}Co_x)_{14}B$. *Journal of Applied Physics*, **64**, 5549.

[5] Xie, J.Q., Wu, C.H., Chuang, Y.C. and Yang, F.M. (1990) Mössbauer Spectra Study of $Nd_2Fe_{14-x}Ga_xB$ and $Nd_2Fe_{11.5-x}Co_{2.5}Ga_xB$ Compounds. *Journal of Applied Physics*, **68**, 4208. https://doi.org/10.1063/1.346210

[6] Harrison, N.J., Davies, H.A. and Todd, I. (2006) $Nd_2Fe_{14}B$-Based Nanocomposite Magnets with Transition Metal and Carbon Additions. *Journal of Applied Physics*, **99**, 08B504-08B504-3. https://doi.org/10.1063/1.2162820

[7] Quan, N., Luo, Y., Yan, W., Yuan, C., Yu, D., Sun, L., Lu, S., Li, H. and Zhang, H. (2017) Hard Magnetic Properties and Coercivity Mechanism of Melt-Spun Misch Metal-Fe-B Alloy. *Journal of Magnetism and Magnetic Materials*, **437**, 12-16. https://doi.org/10.1016/j.jmmm.2017.04.050

[8] Wang, H., Chen, R., Yin, W., Zhu, M., Tang, X., Wang, Z., Jin, C., Ju, J., Lee, D. and Yan, A. (2017) The Effect of Nd-Cu Diffusion during Hot Pressing and Hot Deformation on the Coercivity and the Deformation Ability of Nd-Fe-B HDDR Magnets. *Journal of Magnetism and Magnetic Materials*, **438**, 35-40. https://doi.org/10.1016/j.jmmm.2017.04.031

[9] Yamasaki, M., Hamano, M. and Kobayashi, T. (2002) Mössbauer Study on the Crystallization Process of $\alpha$-Fe/$Nd_2Fe_{14}B$ Type Nanocomposite Magnet Alloy. *Materials Transactions*, **43**, 2885-2889. https://doi.org/10.2320/matertrans.43.2885 http://iss.ndl.go.jp/books/R100000002-I000000163280-00

[10] Hasiak, M., Miglierini, M., Yamashiro, Y., Ciurzynska, W.H., Yanai, T. and Fukunaga, H. (2003) Microstructure and Magnetic Properties of Nanocrystalline Fe-Zr-TM-B-Cu (TM = Nb or Mn) Alloys. *Journal of Magnetism and Magnetic Materials*, **254**, 457-459. https://doi.org/10.1016/S0304-8853(02)00886-7

[11] Girt, E., Krishnan, K.M., Thomas, G., Girt, E. and Altouniam, Z. (2001) Coercivity Limits and Mechanism in Nanocomposite Nd-Fe-B Alloys. *Journal of Magnetism and Magnetic Materials*, **231**, 219-230. https://doi.org/10.1016/S0304-8853(01)00031-2

[12] Hoque, S.M., Hakim, M.A., Khan, F.A. and Dan, N.H. (2007) Effect of Tb Substitution on the Magnetic Properties of Exchange-biased $Nd_2Fe_{14}B/Fe_3B$. *Journal of Material Science*, **42**, 9415-9420. https://doi.org/10.1007/s10853-007-1884-3

[13] Li, L., Tirado, A., Conner, B.S., Chi, M., Elliott, A.M., Rios, O., Zhou, H. and Pa-

ranthaman, M.P. (2017) A Novel Method Combining Additive Manufacturing and Alloy Infiltration for NdFeB Bonded Magnet Fabrication. *Journal of Magnetism and Magnetic Materials*, **438**, 163-167. https://doi.org/10.1016/j.jmmm.2017.04.066

[14] Zhou, C. and Pinkerton, F.E. (2014) Magnetic Hardening of $CeFe_{12-x}Mo_x$ and the Effect of Nitrogenation. *Journal of Alloys and Compounds*, **583**, 345-350. https://doi.org/10.1016/j.jallcom.2013.08.175

[15] Lee, Y.I., Huang, G.Y., Shih, C.W., Chang, W.C. Chang, H.W. and You, J.S. (2017) Coercivity Enhancement in Hot Deformed $Nd_2Fe_{14}B$-Type Magnets by Doping Low-Melting RCu Alloys (R = Nd, Dy, Nd + Dy). *Journal of Magnetism and Magnetic Materials*, **439**, 1-5. https://doi.org/10.1016/j.jmmm.2017.05.009

[16] Withanawasam, L., Murphy, A.S., Hadjipanayis, G.C. and Krause, R.F. (1994) Nanocomposite $R_2Fe_{14}B$/Fe Exchange Coupled Magnets. *Journal of Applied Physics*, **76**, 7065-7067. https://doi.org/10.1063/1.358028

[17] Wecker, J. and Schultz, L. (1987) Beneficial Effect of Co Substitution on the Magnetic Properties of Rapidly Quenched Nd-Fe-B. *Applied Physics Letters*, **51**, 697. https://doi.org/10.1063/1.98339

[18] Miao, W.F., Ding, J., McCormick, P.G. and Street, R. (1996) Structure and Magnetic Properties of Mechanically Milled $Nd_{2x}Fe_{100-3x}B_x$ ($x$ = 2 - 6). *Journal of Alloys and Compounds*, **240**, 200-205. https://doi.org/10.1016/0925-8388(96)02199-8

[19] Tan, G.S., Xu, H., Yu, L.Y., Tan, X.H., Zhang, Q., Gu, Y. and Hou, X.L. (2017) Study on Magnetic Properties of $(Nd_{0.8}Ce_{0.2})_{2-x}Fe_{12}Co_2B$ ($x$ = 0 - 0.6) Alloys. *Journal of Magnetism and Magnetic Materials*, **437**, 17-22. https://doi.org/10.1016/j.jmmm.2017.04.032